Acta Crystallographica Section D
Biological Crystallography
ISSN 0907-4449

The first structure of a cold-active catalase from *Vibrio salmonicida* at 1.96 Å reveals structural aspects of cold adaptation

Ellen Kristin Riise,[a]‡ Marit Sjo Lorentzen,[b]‡ Ronny Helland,[a] Arne O. Smalås,[a] Hanna-Kirsti S. Leiros[a] and Nils Peder Willassen[a,b]*

[a]The Norwegian Structural Biology Centre (NorStruct), Department of Chemistry, Faculty of Science, University of Tromsø, N-9037 Tromsø, Norway, and [b]Department of Molecular Biotechnology, Institute of Medical Biology, Faculty of Medicine, University of Tromsø, N-9037 Tromsø, Norway

‡ These authors contributed equally to this work.

Correspondence e-mail: nilspw@fagmed.uit.no

Received 25 August 2006
Accepted 20 October 2006

PDB Reference: catalase, 2isa, r2isasf.

The cold-adapted catalase from the fish-pathogenic bacterium *Vibrio salmonicida* (VSC) has recently been characterized and shown to be two times more catalytically efficient compared with catalase from the mesophilic human pathogen *Proteus mirabilis* [PMC; Lorentzen *et al.* (2006), *Extremophiles*, **10**, 427–440]. VSC is also less temperature-stable, with a half-life of 5 min at 333 K compared with 50 min for PMC. This was the background for solving the crystal structure of the cold-adapted VSC to 1.96 Å and performing an extensive structural comparison of VSC and PMC. The comparison revealed that the entrance (the major channel) leading to the catalytically essential haem group, is locally more flexible and slightly wider in VSC. This might explain the enhanced catalytic efficiency of the nearly diffusion-controlled degradation of hydrogen peroxide into water and molecular oxygen in VSC. The reduced thermal stability of the cold-adapted VSC may be explained by a reduced number of ion-pair networks. The four C-terminal α-helices are displaced in the structures, probably owing to missing ionic interactions in VSC compared with PMC, and this is postulated as an initiation site for unfolding the cold-adapted enzyme. VSC is the first crystal structure reported of a cold-adapted monofunctional haem-containing catalase.

1. Introduction

Cold-adapted enzymes are generally characterized by a higher catalytic efficiency and a reduced temperature optimum and thermal stability compared with their mesophilic counterparts. A hypothesis presented by Hochachka & Somero (1984) suggested that the reduced stability was probably a consequence of a more flexible structure owing to the need for rapid conformational changes during catalysis at low temperatures. The cold-active enzymes investigated so far seem to have developed different adaptive strategies in order to perform more efficient catalysis in cold environments compared with their mesophilic homologues (Smalås *et al.*, 2000; D'Amico *et al.*, 2002; Russell, 2000; Sheridan *et al.*, 2000). Comparative structural analysis (three-dimensional structures and homology models) has revealed several possible mechanisms for the increase in conformational flexibility of cold-adapted enzymes (Smalås *et al.*, 2000). These include a decrease in the number of intermolecular and/or intramolecular salt bridges, proline or arginine residues and hydrogen bonds. A decrease in the number of bound ions and an increase in their dissociation constants have also been observed. Increased surface charges leading to increased interactions with solvent is another

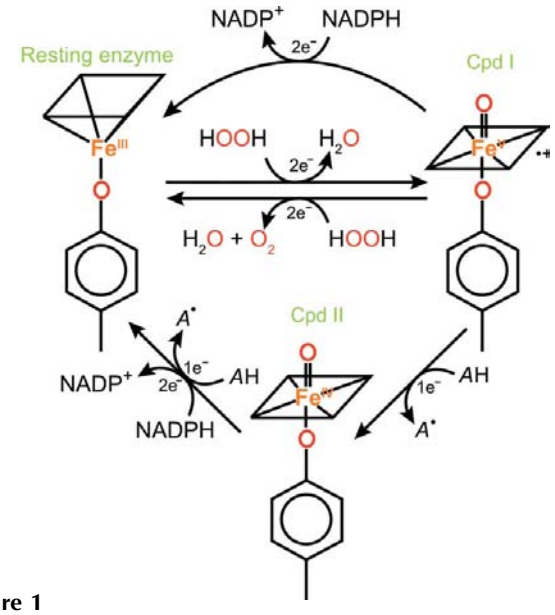

Figure 1
The degradation of hydrogen peroxide is divided into two stages. In the first stage, one hydrogen peroxide molecule oxidizes the haem from the resting state (Fe^{III}) to compound I (Cpd I; a nominal Fe^{V} state). In the second stage, the enzyme is reduced back to the resting enzyme state by a second hydrogen peroxide molecule, releasing water and molecular oxygen. Catalase may also bind NADPH when a steady flow of hydrogen peroxide is supplied, which has been implicated in preventing the accumulation of an inactive partially oxidized dead-end form of the enzyme, Cpd II. NADPH then reduces Cpd I back to the resting state of the enzyme. In the absence or at limited concentrations of H_2O_2 or NADPH, Cpd I can be reduced in a stepwise manner to recover the resting state of the enzyme *via* an intermediate, Cpd II, where the electrons are derived from endogenous donors (*A*H).

observed feature. Furthermore, a reduction in hydrophobicity in the core, the replacement of residues to allow greater rotational freedom and amino-acid substitutions that decrease interdomain interactions in multimeric proteins may be other mechanisms responsible for increased flexibility (Russell, 2000; Sheridan *et al.*, 2000).

Catalases (EC 1.11.1.6) are ubiquitous enzymes found in many different prokaryotic and eukaryotic organisms from all three kingdoms of life. They degrade hydrogen peroxide into water and molecular oxygen and function as a protective response to damage of cellular components (Switala & Loewen, 2002). The catalysis $2H_2O_2 \rightarrow 2H_2O + O_2$ is divided into two stages. The first hydrogen peroxide molecule oxidizes the haem (*via* a two-electron transfer) in the resting-state enzyme to an oxyferryl intermediate, compound I (Cpd I; a nominal Fe^{5+} state). In the second stage, compound I is reduced back to the resting state by another hydrogen peroxide molecule, thus regenerating the resting-state enzyme (an Fe^{3+} state) and releasing water and oxygen (Chelikani *et al.*, 2004; equations 1 and 2; Fig. 1). However, under conditions of a steady flow of hydrogen peroxide or with other hydrogen donors, an additional species, compound II (Cpd II; an Fe^{4+} state), can be formed *via* a one-electron reduction of compound I (equation 3; Fig. 1). Compound II does not react with hydrogen peroxide. Thus, accumulation of compound II leads to inactivation of the enzyme. Some catalases are able to bind NADPH and use this cofactor as protection against inactivation to compound II as long as the NADPH is not oxidized (Hillar *et al.*, 1994; Hillar & Nicholls, 1992; Kirkman *et al.*, 1987).

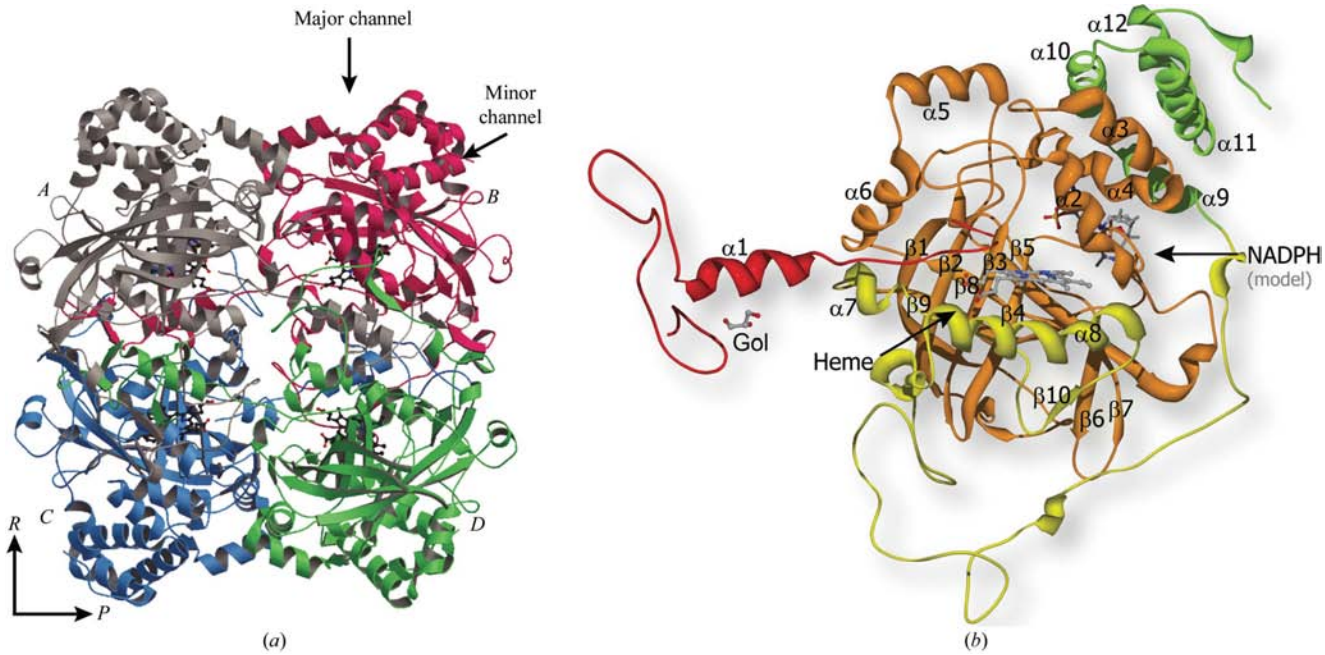

Figure 2
(*a*) Quaternary structure of the VSC tetramer with monomers *A* (grey), *B* (magenta), *C* (blue) and *D* (green). *P*, *Q* and *R* are the molecular axes of the tetramer as described by Fita *et al.* (1986), where the *P* axis is between monomers *A*–*C* and *B*–*D*, the *R* axis is between monomers *A*–*B* and *C*–*D* and the *Q* axis is perpendicular to *P* and *R*. Arrows indicate the major and minor channels. (*b*) Tertiary structure of the VSC monomer generated by *Swiss-PdbViewer* (Guex & Peitsch, 1997), with the N-terminal domain (residues 2–55) in red, the β-barrel domain (residues 56–301) in orange, the wrapping domain (residues 302–416) in yellow and the α-helical domain (417–484) in green. The observed protohaem IX (heme) and the modelled NADPH are coloured light grey.

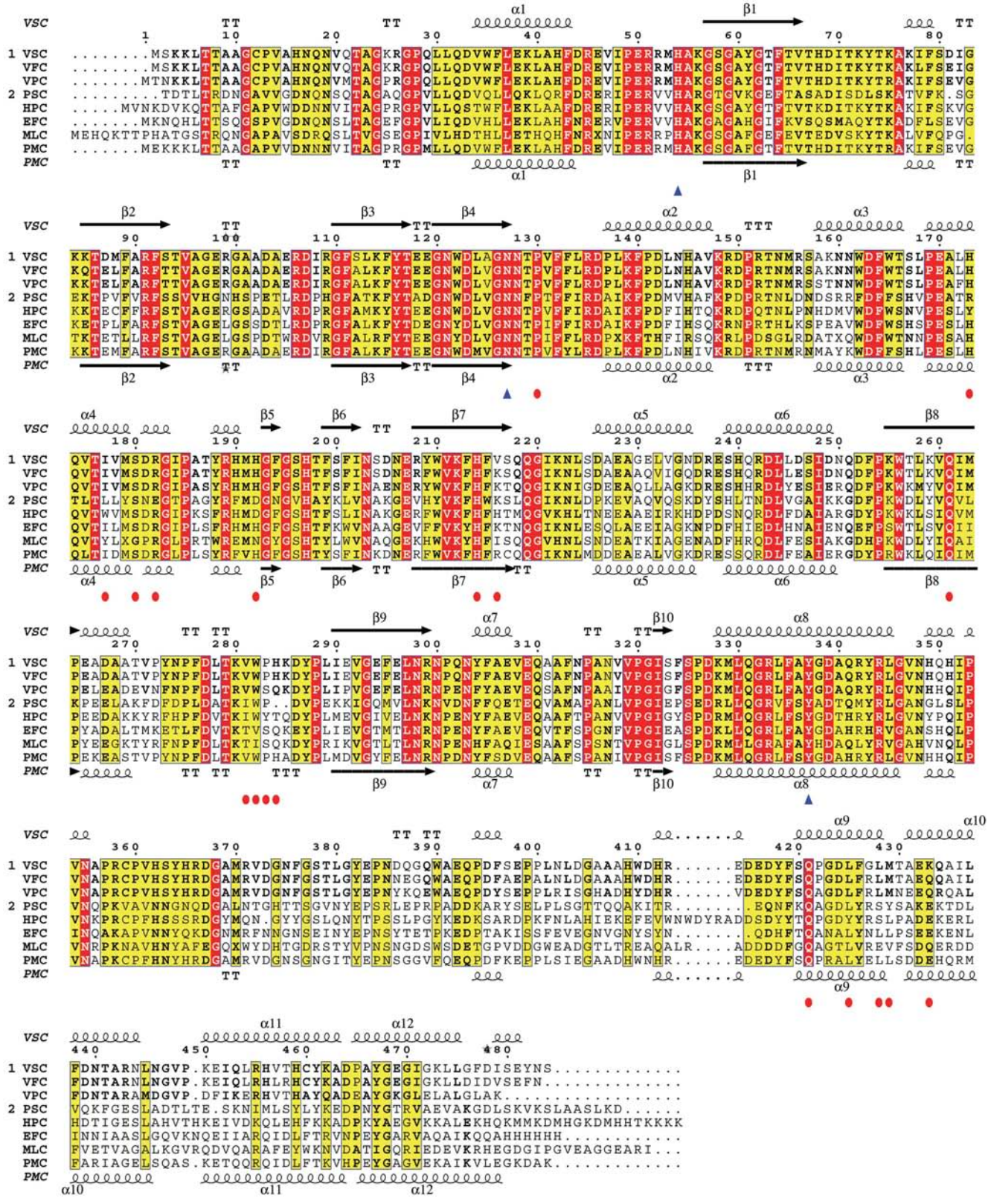

Figure 3
Sequence alignment with the secondary structure of VSC (top) and PMC (bottom). The active-site residues are marked with blue triangles and NADPH-interacting residues are marked with red circles. The sequence abbreviations (species, gene bank entry or PDB codes) are VSC (*V. salmonicida*; ABA26662), VFC (*V. fischeri*; YP_205967), VPC (*V. parahaemolyticus*; BAC62761), PSC (*Pseudomonas syringae*; PDB code 1m7s), HPC (*Helicobacter pylori*; PDB code 1qwl), EFC (*Enterococcus faecalis*; PDB code 1si8), MLC (*Micrococcus luteus*; PDB code 1gwe) and PMC (*Proteus mirabilis*; PDB code 1m85). Conserved residues in VSC, VFC and VPC sequences are outlined in bold in the figure, which was made with *ESPript* v.2.2 (Gouet *et al.*, 1999).

$$\text{Enz (haem-Fe}^{\text{III}}) + H_2O_2 \rightarrow \text{Cpd I (haem-Fe}^{\text{V}}{=}O) + H_2O \quad (1)$$

$$\text{Cpd I (haem-Fe}^{\text{V}}{=}O) + H_2O_2 \rightarrow \text{Enz (haem-Fe}^{\text{III}}) + H_2O + O_2 \quad (2)$$

$$\text{Cpd I (haem-Fe}^{\text{V}}{=}O) + AH \rightarrow \text{Cpd II (haem-Fe}^{\text{IV}}{=}O) + A^{\cdot} \quad (3)$$

Owing to their variety of subunit sizes, number of quaternary structures, different haem prosthetic groups and variety of sequence groups (Nicholls *et al.*, 2001), catalases are divided into three main categories of proteins exhibiting significant catalase activity. These categories are the monofunctional haem-containing catalases, the bifunctional haem-containing catalase-peroxidases and the nonhaem manganese-containing catalases (von Ossowski *et al.*, 1993; Zamocky & Koller, 1999). Haem-containing proteins with minor levels of catalase activity, not considered to be catalases, have been characterized as a fourth category (Maté *et al.*, 2001; Nicholls *et al.*, 2001). The three-dimensional structures of six monofunctional haem-containing catalases of bacterial origin have been determined to date. These are those from *Escherichia coli* HPII (Bravo *et al.*, 1995), *Micrococcus lysodeikticus* (Murshudov *et al.*, 1992), *Proteus mirabilis* (Gouet *et al.*, 1995), *Pseudomonas syringae* (Carpena *et al.*, 2003), *Helicobacter pylori* (Loewen *et al.*, 2004) and *Enterococcus faecalis* (Håkansson *et al.*, 2004). Most monofunctional haem-containing catalases consist of four identical small or large monomers with a molecular weight in the range 50–85 kDa, each with a prosthetic haem group deeply buried in the quaternary structure. The small monomer is composed of four distinct structural domains (Fita & Rossmann, 1985; Melik-Adamyan *et al.*, 1986) as shown in Fig. 2(*b*), whereas the large-monomer enzymes contain an additional flavodoxin-like domain (Zamocky & Koller, 1999).

The tetrameric structure of small-monomer catalases (Fig. 2*a*) includes the interweaving of adjacent monomers, which results in two tightly associated dimers per tetramer. The N-terminal arm of monomer *A* is slipped through the wrapping domain of monomer *B* (Nicholls *et al.*, 2001), resulting in dimerization, while tetramer contacts are present between the wrapping domain of monomer *A* and residues in monomer *C*. The haem environment is defined by residues from all the domains with the exception of the α-helical domain (Zamocky & Koller, 1999).

The small-monomer catalases characterized to date contain haem *b*, while the large-monomer catalases contain a 180° flipped haem *d* in their active site (Nicholls *et al.*, 2001). A tyrosine (Tyr337, VSC numbering) on the proximal side of the haem and a histidine (His54) and an asparagine (Asn127) on the distal side are considered to be essential in catalysis (Maté *et al.*, 2001). Monofunctional haem-containing catalases contain several channels per monomer that extend from the molecular surface to the deeply buried haem groups (Chelikani *et al.*, 2004). A funnel-shaped connection, termed the major channel, of approximately 30 Å (in PMC; Gouet *et al.*, 1995) from the molecular surface to the active site allows access of substrate to the haem group.

Some of the small-monomer catalases have the ability to bind the cofactor NADPH in each monomer (Murshudov *et al.*, 2002; Gouet *et al.*, 1995). The NADPH-binding pocket is located about 20 Å from the haem iron and it seems as if the electron transfer is performed through electron tunnelling (Almarsson *et al.*, 1993; Bicout *et al.*, 1995). A proposed role of NADPH is protection of the enzyme against inactivation of its own substrate (DeLuca *et al.*, 1995; Kirkman *et al.*, 1999), compound II, as shown in Fig. 1.

Recombinant monofunctional haem-containing catalase from the psychrophilic fish pathogen *Vibrio salmonicida* (VSC) has been characterized and shown to be two times more catalytically efficient at 277 K compared with the mesophilic human pathogen *P. mirabilis* (PMC). The higher catalytic efficiency (k_{cat}/K_m) of VSC results from a higher turnover number (k_{cat}) and higher substrate affinity (lower K_m). VSC was also found to be more temperature-labile than PMC with a 19 K lower apparent melting temperature (T_m) (332 *versus* 351 K) and at 333 K the half-life of VSC was less than 5 min, compared with 50 min for PMC. Experimental studies show that VSC binds NADPH (Lorentzen *et al.*, 2006).

The previously observed biochemical differences between VSC and PMC are of particular interest since catalases are known to be almost diffusion-controlled. In this work, we present the crystal structure of VSC at 1.96 Å resolution and a detailed comparison with PMC. Differences in intramonomer and intermonomer interactions were investigated in order to possibly reveal cold-adapted features of VSC on the molecular level.

2. Materials and methods

2.1. Structure determination and model refinement

The protein was purified and crystallized as previously described (Riise *et al.*, 2006), with the best diffracting crystals obtained using the hanging-drop method with reservoir solution containing 2.0 *M* ammonium sulfate, 2% PEG 400 and 100 m*M* Na HEPES pH 7.5 at 293 K. The drops were made by mixing 1 µl protein solution (22 mg ml^{-1}) and 1 µl reservoir solution and the final crystal size was approximately 0.1 × 0.4 × 0.4 mm. 15% glycerol was added to the reservoir solution to obtain the cryoprotectant. Diffraction data were collected at 100 K at the Swiss–Norwegian beamline (BM01A) at the European Synchrotron Radiation Facility (ESRF) to 1.96 Å resolution from crystals belonging to space group $P2_1$ with unit-cell parameters a = 98.15, b = 217.76, c = 99.28 Å, β = 110.48°. With eight monomers in the asymmetric unit, the resulting Matthews coefficient was 2.37 Å^3 Da^{-1} and the solvent content was 48.1%. The phase problem was solved by molecular replacement using the program *Phaser* (McCoy *et al.*, 2005). The search model was PMC (PDB code 1m85), which has 71% sequence identity, with the side chains mutated to fit the VSC sequence (accession No. DQ 182487).

Molecular replacement was followed by one run of rigid-body refinement using all data (20–1.96 Å) and subsequent model refinement in *REFMAC*5 (Murshudov *et al.*, 1997) from

Table 1
Sequence identity (%) and similarity among the monofunctional haem-containing catalase sequences from VSC, VFC, VPC and PMC.

The numbers on the diagonal are the sequence length of the catalase. The values above the diagonal are the sequence identity/sequence similarity (%). The numbers below the diagonal are the number of identical/number of similar residues.

	VSC	VFC	VPC	PMC
VSC	483	93/97	79/88	71/83
VFC	452/473	482	80/89	70/84
VPC	386/430	389/431	479	69/82
PMC	344/404	341/408	335/401	484

Table 2
Composition (selected amino acids) of the monomers of VSC and PMC.

Residues were distributed into the groups E (external) and I (internal) (as described in §2). The theoretical pI was calculated from the full-length sequences. Residues included in the various class definitions are net charged (KRDE), charged (RKHDE), acidic (DE), basic (KRH), polar (QNCSTYRKHDE), hydrophobic (AILFWVPM) and aromatic (FWY). The ratios Arg/(Arg + Lys) and (Ile + Leu)/(Ile + Leu + Val) are also shown.

	VSC			PMC		
Classes	E	I	Total	E	I	Total
pI (calculated)			5.92			6.11
Net charge			−11			−10
Charged	104	31	135	114	31	145
Acidic	49	14	63	51	17	68
Basic	55	17	72	63	14	77
Polar	171	75	246	176	75	251
Hydrophobic	84	110	194	82	110	192
Aromatic	27	27	54	26	31	57
Amino acids			483			484
Ala (A)	21	19	40	16	18	34
Glu (E)	21	5	26	28	5	33
Gly (G)	13	23	36	13	20	33
Met (M)	2	7	9	6	7	13
Pro (P)	19	10	29	18	11	29
Arg (R)	23	4	27	28	4	32
Arg/(Arg + Lys)			0.52			0.55
(Leu + Ile)/(Leu + Ile + Val)			0.66			0.66

the *CCP*4 suite (Collaborative Computational Project, Number 4, 1994), with manual building in *O* (Jones *et al.*, 1991) according to $F_o - F_c$ and $2F_o - F_c$ electron-density maps. The quality of the process was assessed by the use of R_{free} statistics for 5% of the reflections. The eight monomers in the asymmetric unit were not coupled by noncrystallographic symmetry (NCS) and were refined separately throughout the refinement of the structure. Water molecules with peaks of at least 3.5σ in $F_o - F_c$ maps and with distances of 2.2–3.7 Å to hydrogen-bonding partners were added by the *ARP_WATERS* routine within *REFMAC*5 (Murshudov *et al.*, 1997) from *CCP*4 (Collaborative Computational Project, Number 4, 1994).

The final model was validated by *PROCHECK* (Laskowski *et al.*, 1993) and *SFCHECK* (Vaguine *et al.*, 1999). See Table 3 for more details.

2.2. Homology model building

The modelled structures of the *V. fischeri* (VFC; accession No. YP 205967) and *V. parahaemolyticus* (VPC; accession No. NP 800928) catalases were made by homology modelling using *Swiss-PdbViewer* (Guex & Peitsch, 1997). The crystal structure of a VSC tetramer was used as a template to generate tetrameric models of VFC and VPC. Sequence alignment was performed using *ClustalW* (Thompson *et al.*, 2000).

2.3. Structural comparison

For simplicity, the VSC structure was numbered identically to PMC, starting with Met2. In the PMC model the N- and C-terminal residues 1–3 and 480–484, respectively, were excluded from the structural comparison owing to their absence in the crystal structure. Classification of internal and external residues was based on the water-accessible surfaces found in the tetrameric PMC structure using *DSSP* (Kabsch & Sander, 1983). Residues with water-accessible surfaces larger than 10 Å^2 were defined as external (E) and the others as internal (I).

2.4. Analysis of structural features

In the structural analysis, the amino-acid numbering refers to the VSC structure.

The program *Swiss-PdbViewer* (Guex & Peitsch, 1997) was used to estimate the cavity volume in the major channel adjacent to the haem group. Since the channel is exposed to solvent, the volume is hard to measure in the original structure; therefore, we closed the channel by placing two antiparallel β-strands (a total of 19 residues) over the entrance in the vicinity of residues 147, 161, 179 and 444 and almost parallel to the haem group. This was performed for VSC and for PMC superimposed onto VSC. The volumes between the haem group and the two β-strands were then estimated.

Salt bridges were calculated using the *WHAT IF* web interface (Vriend, 1990) between negatively charged atoms (side-chain O atoms in Asp or Glu) and positively charged atoms (side-chain N atoms in Arg, Lys or His) with an interatomic distance of <4 Å or <6 Å. Histidines were considered to be positively charged. An ion pair was defined as the interaction between opposite charged residues; thus, each individual residual interaction (single ion pair) was counted, as described previously (Gianese *et al.*, 2002).

Hydrogen bonds were calculated using the program *HBPLUS* v.3.15 (McDonald & Thornton, 1994) with the following parameters for donor (D), acceptor (A), acceptor antecedents (AA) and (calculated) hydrogen (H) atoms: maximum distances for D—A, 3.5 Å, H—A, 2.5 Å; minimum angle for D—H—A, D—A—AA and H—A—AA of 90°. All ion pairs were included in the calculations. The results were evaluated using *Swiss-PdbViewer* (Guex & Peitsch, 1997).

The surface images were created with *PyMOL* (DeLano, 2002) and edited with *Adobe Photoshop*.

3. Results and discussion

3.1. Amino-acid composition and distribution

In order to identify the amino-acid residues responsible for the observed cold-adapted features of VSC, the sequences of

VSC and PMC were aligned and compared (Fig. 3). The alignment also includes the psychrotrophic *V. fischeri* catalase (VFC) and the mesophilic *V. parahaemolyticus* catalase (VPC) in order to verify trends among the psychrophilic, psychrotrophic and mesophilic catalases within the *Vibrio* genus (Fig. 3) and thus focus on residues possibly involved in cold adaptation. The sequence was also compared with the amino-acid sequences from other catalase structures, but since we have previously performed comparative kinetic studies of VSC and PMC (Lorentzen *et al.*, 2006), we focus our further comparison on these two catalases.

VSC, VFC, VPC and PMC consist of 483, 482, 479 and 484 amino acids, respectively, and the sequence identity among the *Vibiro* enzymes is 79–93%; the *Vibrio* enzymes and PMC have 69–71% identity, as shown in Table 1 and Fig. 3. The sequence identity in the C-terminal part of the VSC and PMC sequences, especially in the α-helical domain (residues 417–484), is considerably lower than in the other domains.

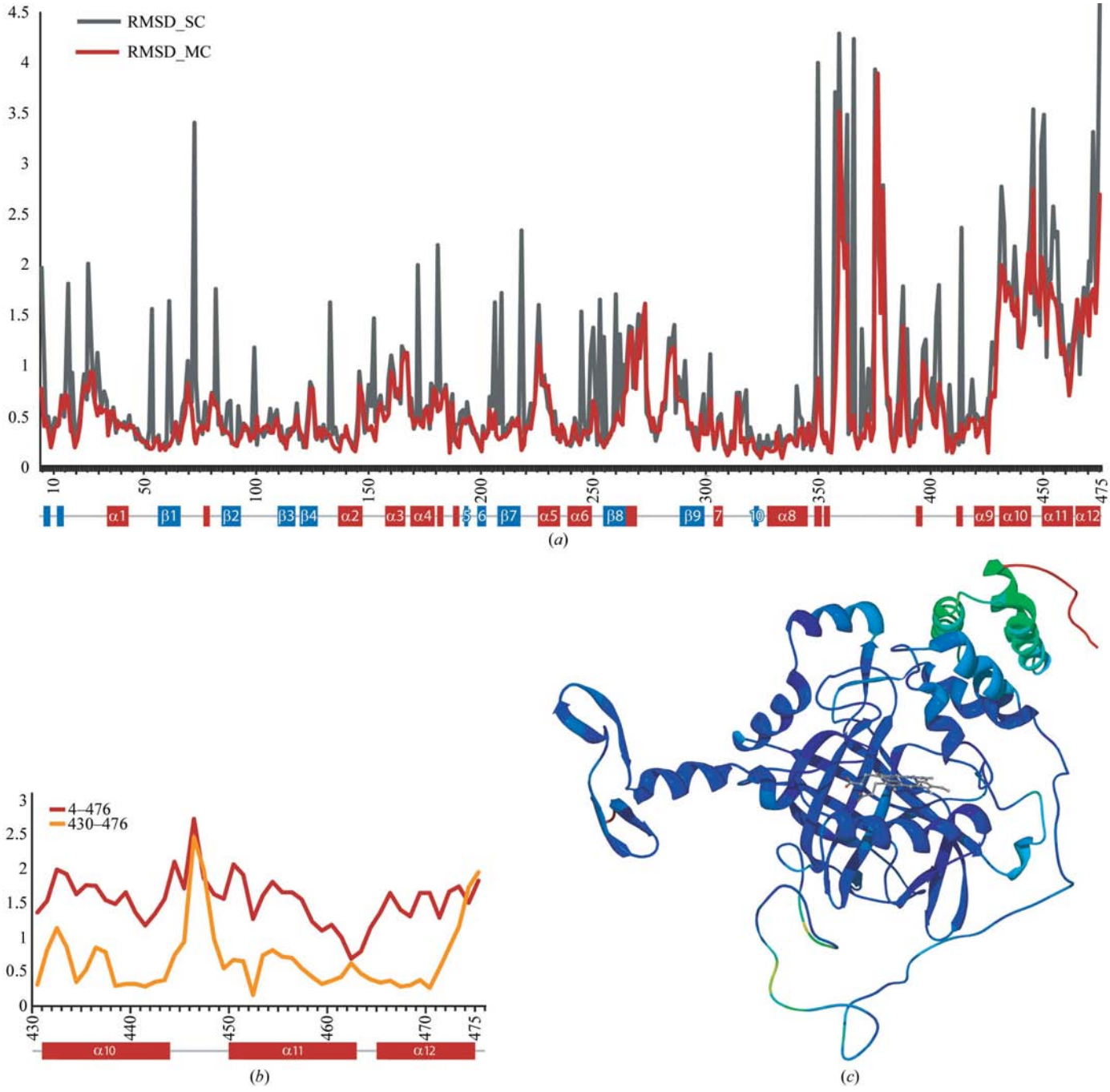

Figure 4
Superpositioning of VSC onto PMC. (*a*) Residue-averaged r.m.s. deviation for residues 4–476 when main-chain (red; RMSD_MC) and side-chain (grey; RMSD_SC) atoms were compared. (*b*) Superpositioning of VSC onto PMC using only residues 430–476 (yellow) in the superposition and the r.m.s. deviation when all residues (4–476; red) were included. (*c*) The VSC monomer coloured by r.m.s. deviations compared with PMC. Dark blue represents good superposition, whereas red represents poor superposition.

Table 3
Data-collection and refinement summary.

Values in parentheses are for the outer shell.

Data collection	
Resolution range (Å)	25–1.96 (2.06–1.96)
No. of unique reflections	267579
Multiplicity	2.6 (2.5)
R_{merge} (%)	11.1 (36.1)
Completeness (%)	95.9 (83.3)
Average $I/\sigma(I)$	6.0 (2.0)
Wilson B factor (Å^2)	16.8
Refinement statistics, all atoms (chains A–H)	
R value (%)	14.8
Free R value (%)	20.0
Deviation from ideal geometry	
Bond lengths (Å)	0.010
Bond angles (°)	1.268
Average B values (Å^2)	
Main-chain atoms (15264)	12.6
Side-chain atoms (20744) and waters (4594)	15.9
Haems (8)	8.1
Glycerols (8)	12.1
Chloride ions (4)	15.5
All atoms	14.0
Ramachandran plot (%)	
Most favoured regions	87.7
Additional allowed regions	11.6
Generously allowed regions	0.2 (Asp367)
Disallowed regions	0.5 (Tyr364, Ser196)

Table 4
Hydrogen bonds and distances (Å) (in parentheses) involving the haem group in VSC and PMC.

For PMC, His341 in the original PDB file is oriented so that no hydrogen bonds are formed to the haem group, but if the χ_1 angle is rotated 180° there is a hydrogen bond from His341 NE1 to Haem O1A.

		VSC				PMC
		Mol. *A*	Mol. *B*	Mol. *C*	Mol. *D*	Mol. *A*
Arg51 NE	Haem O2D	2.81	2.74	2.74	2.78	2.82
Arg91 NH1	Haem O1D	2.77	2.79	2.67	2.71	2.86
Gln341 NE2	Haem O1A	2.98	2.84	3.05	2.98	
His341 NE2	Haem O1A					(3.25)
Arg344 NE	Haem O2A	2.76	2.78	2.83	2.81	2.79
Arg344 NH2	Haem O1A	3.06	2.8	2.96	2.88	2.80
Tyr337 OH	Haem Fe	1.95	1.78	1.82	1.90	2.05
His54 NE2	W1	2.75	2.63	2.74	2.56	2.84
W1	Haem Fe	(3.81)	(4.12)	(4.10)	(4.22)	3.46
W2	Haem O1A	2.88	2.74	2.77	2.77	2.70
W3	Haem O2A	2.52	2.77	2.48	2.71	2.69
W4	Haem O1D	2.79	2.59	2.80	2.65	2.76
W2	Haem O2D	2.70	2.74	2.83	2.66	2.72

The most striking difference in amino-acid composition between VSC and PMC is the lower number of charged external residues in VSC compared with PMC (135 and 145, respectively). There are 27 and 32 Arg residues in VSC and PMC, respectively, of which 25 are conserved (Table 2). This results in a lower Arg/(Arg + Lys) ratio, which is considered to be a cold adaptation feature, in VSC. The total number of hydrophobic (AILFWVPM) residues is slightly higher in VSC, mostly owing to additional Ala residues. The number of internal Ile residues in VSC is somewhat lower compared with PMC, whereas the opposite applies for Leu. VSC contains fewer Met residues (nine) than PMC (13), differing from many other cold-adapted enzymes, which have more Met than their mesophilic homologues (Gudmundsdottir *et al.*, 1996; Smalås *et al.*, 2000). VSC and PMC possess 30 conserved Gly residues and seven and four unique Gly residues, respectively.

3.2. Overall structure

The crystal structure of VSC was determined to 1.96 Å resolution by molecular replacement using the crystal structure of PMC as a search model with the side chains mutated in order to fit the sequence of VSC. The final R factor is 14.8% and R_{free} is 20.0% (Table 3). The final model of VSC includes eight monomers (denoted A–H) in the asymmetric unit, where only the first Met residue is missing from the electron density. Each monomer contains 482 residues. In addition, eight haems, eight glycerol molecules, four chloride ions and 4637 water molecules are included in the model, which contains approximately 36 000 non-H atoms. The average B factor of all atoms is 14.0 Å^2.

An analysis of the main-chain geometry with a Ramachandran plot shows that 87.7% of all the residues are in the most favourable regions and 11.6% are in additionally allowed regions. Three nonglycine residues are in the generously allowed region and Ser196, Tyr364 and Asp367 are in the disallowed regions for each monomer. The latter residues are all well defined in the electron-density map. Ser196 is also modelled with unfavourable φ/ψ angles in PMC, beef liver catalase (BLC) and *Penicillium vitale* catalase (PVC; Gouet *et al.*, 1995; Fita *et al.*, 1986). Ser196 is located on the haem-proximal side and is suggested to be involved in the electron-transfer mechanism from NADPH to the haem (Bicout *et al.*, 1995).

The structure is in general very well defined in the $2F_o - F_c$ electron-density map. The coordinate error estimated from the Luzzati plot (Luzzati, 1952) is 0.16 Å and Cruickshank's dispersion precision indicator for coordinate error is 0.15 Å. A few residues are modelled with alternative conformations. In chains A–F, residues Arg99 and Gly100 are modelled with two alternative conformations for the main chain. In the first conformation there is a hydrogen bond from Gly100 N of chain A to Arg99 O of chain B and in the second conformation there is a hydrogen bond from Arg99 O of chain A to Gly100 N of chain B. This is similar for all the other dimers.

3.3. Tetrameric structure

VSC forms two tetramers per asymmetric unit. The overall shape of the tetramer is shown in Fig. 2(*a*). The average B factor of all atoms for the tetramers *ABCD* and *EFGH* are 11.59 and 14.27 Å^2, respectively. The r.m.s. deviation between the two tetramers in the asymmetric unit is 0.145 Å for main-chain atoms and 0.205 Å for side-chain atoms, indicating high similarity, with an r.m.s. deviation close to the coordinate error of 0.16 Å (from a Luzzati plot). Therefore, the choice of using

only the *ABCD* tetramer for the structural comparison should be reasonable.

PMC has only one molecule in the asymmetric unit and the tetramer is formed by the $P6_222$ crystal symmetry. Distances and structural comparison are therefore made for monomer *A* or one tetramer of PMC. The rotamer of Met*53 in the deposited PMC structure does not form a hydrogen bond to Asn114 ND2 as described by Gouet *et al.* (1995). Therefore, a 60° rotation in χ_3 was modelled and used throughout this study.

3.4. Monomeric structure

The individual VSC monomers within the *ABCD* tetramer display no significant r.m.s. deviations when compared with each other. The r.m.s. deviation between monomer *A* and monomers *B*–*H* varied from 0.11 to 0.15 Å for main-chain atoms. The average *B* factors of the *A*, *B*, *C* and *D* chains are 11.45, 11.91, 10.87 and 12.12 Å^2, respectively.

The catalase monomer is composed of four domains (Fig. 2*b*). Both the N-terminal arm (residues 2–55), which is highly conserved amongst catalases, and the β-barrel domain (residues 56–301) of VSC reveal no conformational deviation from PMC (see Figs. 4*a*, 4*b* and 4*c*). The wrapping domain (residues 302–416) contains two loop regions with r.m.s. deviations above 3.0 Å for the main chain (see Figs. 4*a*, 4*b* and 4*c*). These residues are involved in the interactions between the dimers and may affect the intermolecular stability. Parts of the C-terminal α-helical domain (residues 417–484) are different in VSC compared with PMC (Figs. 4*a*, 4*b* and 4*c*). The bundle of helices (α9–α12) in this domain is displaced by around 1.5 Å relative to PMC (Fig. 4*b*) starting at residue 430. VSC lacks several ion-pair interactions found in PMC between the helices and the rest of the monomer (Fig. 4). This will be described in more detail later.

3.5. Haem binding

Haem molecules are the major structural component of the active site and are the principal determinant of the activity and specificity of catalases. Each VSC monomer includes one haem molecule, which is oriented in a similar manner to other small-monomer catalases (Carpena *et al.*, 2003), with the active-site His54 oriented above ring III. In both VSC and PMC the haem propionate groups interact with three arginine residues (Arg51, Arg91 and Arg344) and three water molecules (W2, W3, W4) all at similar distances (Table 4). The haem in VSC is further stabilized by a hydrogen bond to Gln341, whereas in PMC this interaction is replaced by an ion pair from His341 NE2 to haem O1A. The ion pair in the latter might bind the prosthetic group more tightly to PMC compared with the hydrogen bond found in VSC.

In the active site at the proximal side of the haem group, there are only a few residue substitutions between VSC and PMC. These are (PMC in parentheses) Ala125 (Val), Phe199 (Tyr), Gln341 (His) and Ala336 (Ser) (Table 5). Position 125 is Val in VFC and VPC, while Phe199, Gln341 and Ala336 are common to the three compared *Vibrio* species. At position 341, PMC forms a hydrogen bond to Phe313 O (3.0 Å) which corresponds to the hydrogen bond from Glu341 NE2 to Phe313 O (2.9 Å) in VSC. PMC has a unique hydrogen bond from Ser336 OG to Asp44*B* OD1 (2.9 Å) in the residues flanking the haem-binding site (Fig. 5). This bond tightens the interactions between monomer *A* and monomer *B* and imposes a lower degree of freedom on the adjacent catalytic residue Tyr337 in PMC; VSC has Ala at position 336 and no interactions at this site. Tyr199 OH in PMC makes one water-mediated hydrogen bond to Arg333 NH1. This is not found in VSC owing to the presence of Phe199. Asn314 ND2 in VSC interacts with Ala316 N, an interaction not present in PMC owing to the presence of Ser in position 314. There are also fewer space-filling residues in VSC (Ala125 and Phe199) compared with PMC (Val125 and Tyr199).

Table 5
Positions possessing different amino acids in the major channel of VSC and PMC.

Level I denotes the entrance of the channel and level V the hydrophobic neck close to the haem group at the bottom of the channel as defined by Fita & Rossmann (1985). nd, not determined. Residues involved in several channel levels are indicated in italic.

Residue position	VSC	PMC	Secondary structure	Channel level
227	Ala	Asp	α6	I
436	Ile	Arg	α11	I
439	Asp†	Ala	α11	I
446	Asn	Ser	Loop	I
477	Phe	Val	α13	I
478	Asp	Leu	α13	I
479	Ile	Glu	nd	I
231‡	Glu	Ala	α6	I
184	Ile†	Leu	Loop	II
230	Gly	Glu	α6	II
440	Asn†	Arg	α11	II
443	Arg†	Gly	α11	II
444	*Asn*	*Glu*	*α11*	*II*
447	Gly†	Gln	Loop	II
235‡	Asn	Lys	α6	II
157	*Ser†*	*Asn*	*Loop*	*III*
158	Ala	Met	α4	III
161	Asn†	Lys	α4	III
165	Trp†	Phe	α4	III
178	*Val†*	*Asp*	*α5*	*III*
444	Asn	Glu	α11	III
146	Ala†	Ile	α3	IV
157	Ser†	Asn	Loop	IV
160	Asn†	Tyr	α4	IV
133	Phe†	Tyr	Loop	V
175	Val†	Leu	α5	V
178	Val†	Asp	α5	V

† Residues that are identical for all three *Vibrio* species. ‡ *R*-related monomer residue.

3.6. Active site

The orientation of the active-site residues His54, Ser93 and Asn127 is almost identical in VSC and PMC, but the water molecule W1 is slightly displaced in PMC, resulting in a longer distance to His54 NE2 (2.8 Å) and a shorter distance to the Fe atom (3.5 Å) compared with VSC (Table 4).

The methionine at position 53 in VSC appeared to be oxidized when inspecting the electron-density maps. Met*53, a

Table 6
Total number of ionic interactions in the crystal structures of VSC and PMC and in the models of VFC and VPC.

A, monomer; *AB*, monomers *A*–*B*; *AC*, monomers *A*–*C*; *AD*, monomers *A*–*D*. 'Ion pairs' denotes ionic interactions between two residues. '3 residues' denotes a three-residue ion-pair network *etc*.

	A	*B*	*C*	*D*	*AB*/*CD*	*AC*/*BD*	*AD*/*BC*	Total
VSC								
<6 Å								
Ion pairs	56	56	57	57	24/25	6/5	8/8	283
3 residues	8	6	9	8	4/4	—	—	39
4/5/6/7/8/9/10 residues	4/1/—/1/1/—/—	5/1/—/1/1/—/—	4/2/—/—/1/—/—	4/1/—/1/1/—/—	—/1 (4)	—	—	18/5/—/3/4—/—
No. of residues	80	74	80	79	88	22	32	455
<4 Å								
Ion pairs	27	26	28	27	20/20	2/2	4/4	160
3 residues	4	4	4	3	2/2	—	—	19
4/5 residues	2/—	2/—	2/—	2/—	—	—	—	8/—
No. of residues	44	42	46	45	76	8	16	277
VFC								
<6 Å								
Ion pairs	57				24/24	8/8	6/6	304
3 residues	6				2/2	—		28
4/5/6/7/8/9/10 residues	5/1/—/—/1/1/—				—	—	—	20/4/—/—/4/4/—
No. residues	80				88	32	24	464
<4 Å								
Ion pairs	28				20/20	2/2	2/2	160
3 residues	4				—	—	—	16
4/5 residues	2/—				—	—	—	8/—
No. residues	46				76	8	8	276
VPC								
<6 Å								
Ion pairs	64				24/24	8/8	6/6	332
3 residues	8				6/6	—	—	44
4/5/6/7/8/9/10 residues	3/1/—/1/1/—/—				—	—	—	12/4/—/4/4/—/—
No. residues	83				84	32	24	472
<4 Å								
Ion pairs	29				18/18	4/4	2/2	164
3 residues	3				—	—	—	12
4/5 residues	2/—				—	—	—	8/—
No. residues	50				68	16	8	292
PMC								
<6 Å								
Ion pairs	73				24/24	6/6	6/6	360
3 residues	8				4/4	—	—	40
4/5/6/7/8/9/10 residues	1/3/—/2/—/1/1				—	—	—	8/12/—/4/—/4/4
No. residues	89				84	24	24	488
<4 Å								
Ion pairs	33				16/16	2/2	2/2	178
3 residues	3				2/2	—	—	16
4/5 residues	2/1				—	—	—	8/4
No. residues	58				60	8	8	308

methionine sulfone also reported and confirmed in PMC (Buzy *et al.*, 1995; Gouet *et al.*, 1995), is located at the end of the major channel at the distal side of the haem. Position 53 is reported as Met in VFC and VPC, but is replaced by a valine in many other catalases (Gouet *et al.*, 1995). The orientation of Met*53 in VSC and PMC is such that a hydrogen bond is formed from one of the side-chain O atoms to Asn114 ND2. The role of this residue is unclear, but since it is inside the major channel it may affect the channel properties.

The slightly higher turnover (k_{cat}) of VSC compared with PMC at 277 K (Lorentzen *et al.*, 2006) might be explained by the loss of a hydrogen bond from monomer *A* (Ser336 OG) to monomer *B* (Asp44 OD1), the presence of only one hydrogen bond from Gln341 to the haem propionate group and fewer space-filling residues at the proximal side of the haem group in VSC compared with PMC. The only residue unique to VSC compared with VFC and VPC is Ala125. Therefore, further investigations such as mutational studies are needed to obtain further insight into the catalytic efficiency of VSC.

3.7. Major channel

The major channel is oriented perpendicular to the haem plane on the distal side and is considered to be the primary access route to the prosthetic group for hydrogen peroxide (Amara *et al.*, 2001; Kalko *et al.*, 2001) and the exit channel for the products. The channel is divided into levels I–V as defined by Fita & Rossmann (1985), where level V is at the bottom of the channel closest to the haem. Substituted residues in VSC compared with PMC in the major channel are given in Table 5. In general, the backbone conformation of the two enzymes is similar in this region, except for the C-terminal residues 474–484, which are folded away from the channel in VSC, and residues 474–479 in PMC, which are oriented towards the

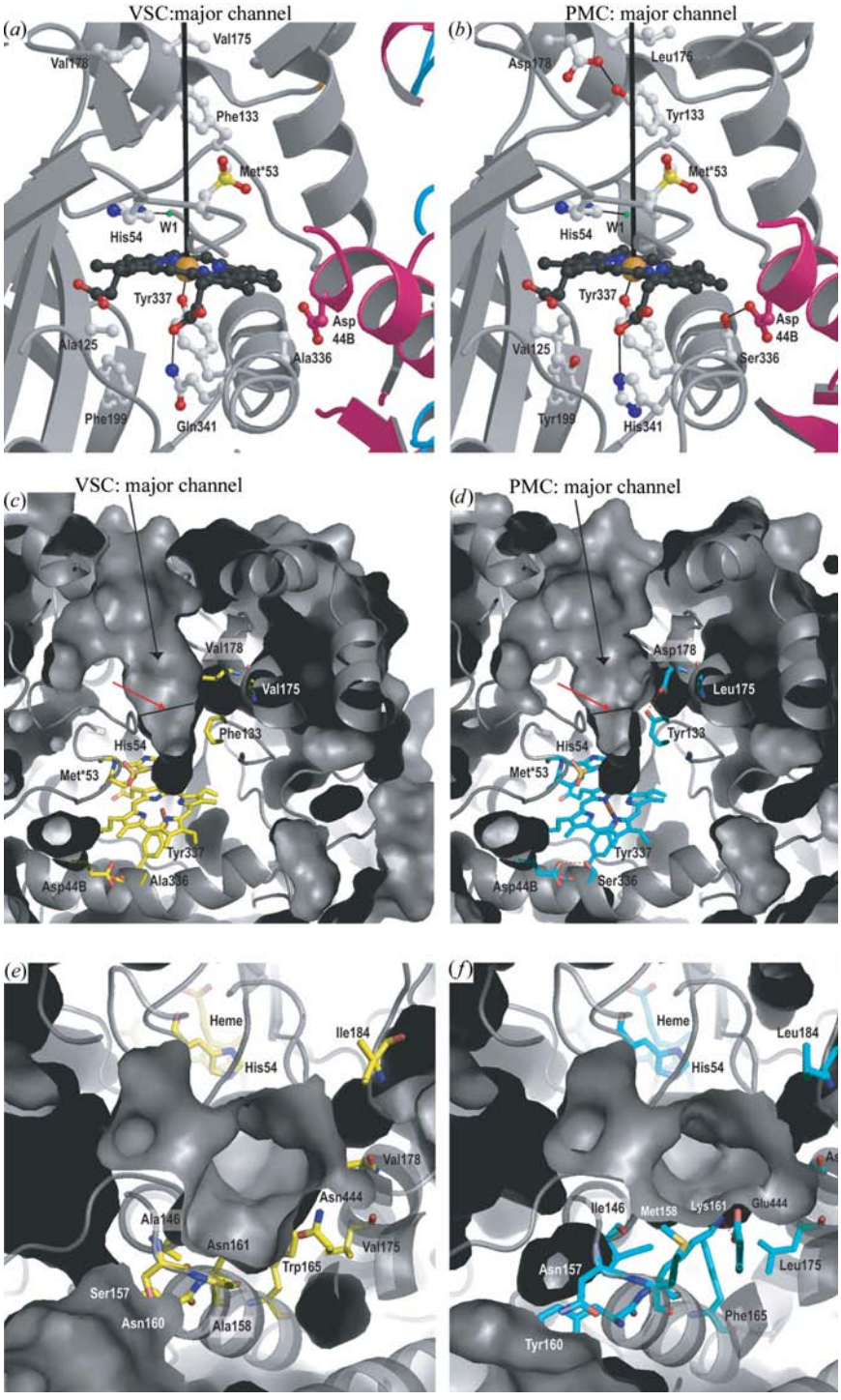

Figure 5
Haem binding in VSC (left panels) and PMC (right panels) using the same orientation for the two enzymes. (*a*, *b*) Positions possessing different amino acids in VSC and PMC. Monomer *A* is coloured grey and monomer *B* magenta. The direction of the channel is indicated by the bold line, whereas hydrogen bonds and ion pairs are illustrated with thinner black lines. (*c*, *d*) Side view of the sliced water-accessible surfaces of VSC and PMC major channels. The width of the major channel leading down to the active site and the haem group is indicated with a black line and a red arrow and is found to be wider in VSC than in PMC. Hydrogen bonds and ion pairs are illustrated with red dotted lines. The direction of the channel is indicated by the black line. (*e*, *f*) Top view of the major channel entrances of VSC and PMC. The channel is more open in VSC mainly owing to the residues (PMC in parentheses) Ala146 (Ile), Ala158 (Met), Asn161 (Lys), Val175 (Leu), Val178 (Asp) and Asn444 (Glu). Hydrogen bonds and ion pairs are illustrated with red dotted lines. See text for further details.

entrance of the channel. This makes the entrance wider in VSC and may allow easier access of the substrate and easier release of the product.

Of special interest are the differences closest to the haem pocket, levels III–V (Table 5). VSC has only hydrophobic residue substitutions at level V (Phe133, Val175, Val178), whereas PMC has Tyr133, Leu175 and Asp178 (Figs. 5*a* and 5*b*). Tyr133 OH is hydrogen bonded to Asp178 OD2 in PMC. Both side chains are within 12–14 Å of the Fe atom in the haem group and these polar or negatively charged residues might affect the catalytic reaction rate. There are no differences in the amino-acid sequence at level IV and V between VSC, VFC and VPC.

The side chains of residues 157 and 160 at level III point out of the channel and residue 146 lines the channel (Figs. 5*e* and 5*f*). These substitutions are expected to have less effect on the channel properties. Ala146 is in the vicinity of Trp165 in VSC (Ile146 and Phe165 in PMC).

There are one positively charged (Lys161) and two negatively charged (Asp178, Glu444) residues in PMC for levels III–V and there is an ion-pair interaction from Lys161 to Glu444 (2.8 Å; Fig. 5*f*). VSC has no charged residues at these positions, only two polar residues (Asn161 and Asn444) and one hydrophobic residue (Val178), and no hydrogen bond from residue 178 to 133 (Table 5). The program *Swiss-PdbViewer* calculated the cavity between the haem group and level I in the channel to be larger in VSC (110 Å^3) than in PMC (60 Å^3). The resulting effect in PMC might be that there are more polar and charged atoms that could bind and be a hindrance for the substrate/product, one hydrogen bond and one ion pair that reduce the flexibility and less space for substrate/product, resulting in a lower reaction rate for catalysis by the mesophilic enzyme.

Our ongoing biochemical studies of NADPH binding to VSC and PMC will present the minor channel differences and properties of the two enzymes and this is therefore not presented here.

3.8. Ionic interactions

A comparative study of 21 psychrophilic enzymes and 427 mesophilic/thermophilic homologues performed by Gianese *et al.*

(2001) suggested that decreased ion-pair interactions and side-chain hydrogen bonds are common adaptive mechanisms of enzymes to low temperatures. A significant decrease in the number of intrasubunit (within the monomer) ion pairs and ion-pair networks is observed in malate dehydrogenase from *Aquaspirillium arcticum* (Kim *et al.*, 1999) and citrate synthase from an Antarctic bacterium (Russell *et al.*, 1998). Therefore, to obtain insight into the protein stability of VSC and PMC, differences in ion pairs and hydrogen bonds have been compared.

The most stable ion pairs are clearly found at a 4 Å cutoff; however, networks and potential ion pairs can still can be detected with a 6 Å cutoff and are therefore included in this study.

The total numbers of observed ion-pair interactions shorter than 4 Å (<6 Å) for one monomer of VSC are 26–28 (56–57) and for PMC are 33 (73) (Table 6). The VSC tetramer has a total of 18 fewer ion pairs than PMC, three more three-residue ion-pair networks and four fewer five-residue ion-pair networks with distances shorter than 4 Å. The total numbers of ion-pair interactions of one monomer of the VFC and VPC models are 28 (57) and 29 (64).

VSC has one unique three-residue ion-pair network <4 Å per monomer (Asp226–Arg443–Asp439), connecting α10 in the α-helical domain to α5 in the β-barrel domain. PMC has one unique ion pair (Lys161–Glu444) in addition to one unique five-residue ion-pair network (Arg106–Asp226–Arg440–Asp181–Arg436), generating a considerably stronger interaction between the two domains (Figs. 6*a* and 6*b*). The difference in ionic interactions may explain the displacement of the α-helices α9–α12 of VSC compared with PMC and hence the reduced stability of VSC compared with PMC.

VSC has one unique ion pair between the wrapping domain and the β-barrel domain (Asp87–Arg358), which is probably responsible for the different conformation of the wrapping loops. The models of VFC and VPC indicate an equivalent ion pair for Glu87–Arg358.

At a 6 Å cutoff, VSC has 17 unique ion pairs, of which ten are present in VFC and VPC, while PMC has 33 unique ion pairs. In addition, VSC has two unique three-residue ion-pair networks, while PMC has five unique three-residue networks and one unique seven-residue ion-pair network. These networks mainly strengthen the interactions between the α-helical domain and the β-barrel domain. The seven-residue ion-pair network in PMC is an extension of the two three-residue networks found in VSC. Residues Glu433 and Arg440 in PMC (Fig. 6*b*) in particular seem to have an important part in the network. These residues are replaced by Lys and Asn in VSC and Gln and Asn in VFC and VPC, respectively, and do not seem to be involved in any ionic interactions.

VSC has one eight-residue ion-pair network <6 Å per monomer connecting the β-barrel domain and the α-helical domain. This is expanded to a ten-residue ion-pair network in PMC. The two extra residues (Asp136 and Lys328) in PMC may increase the strength of the network, but they are also present as a single ion pair in VSC. The seven-residue network in VSC is expanded in PMC by two residues (Asp107 and Arg109), forming a nine-residue ion-pair network. Half of the ionic interactions in PMC are within the β-barrel domain and one is found in the wrapping domain, whereas the rest are between the β-barrel domain and the α-helical domain. The C-terminal α-helices and the wrapping domain of PMC appear to be packed closer to the β-barrel domain and stabilize the monomer, thus indicating higher rigidity of the PMC monomer compared with VSC. A larger number of ion-pair interactions are also found in the VFC and VPC models compared with VSC,

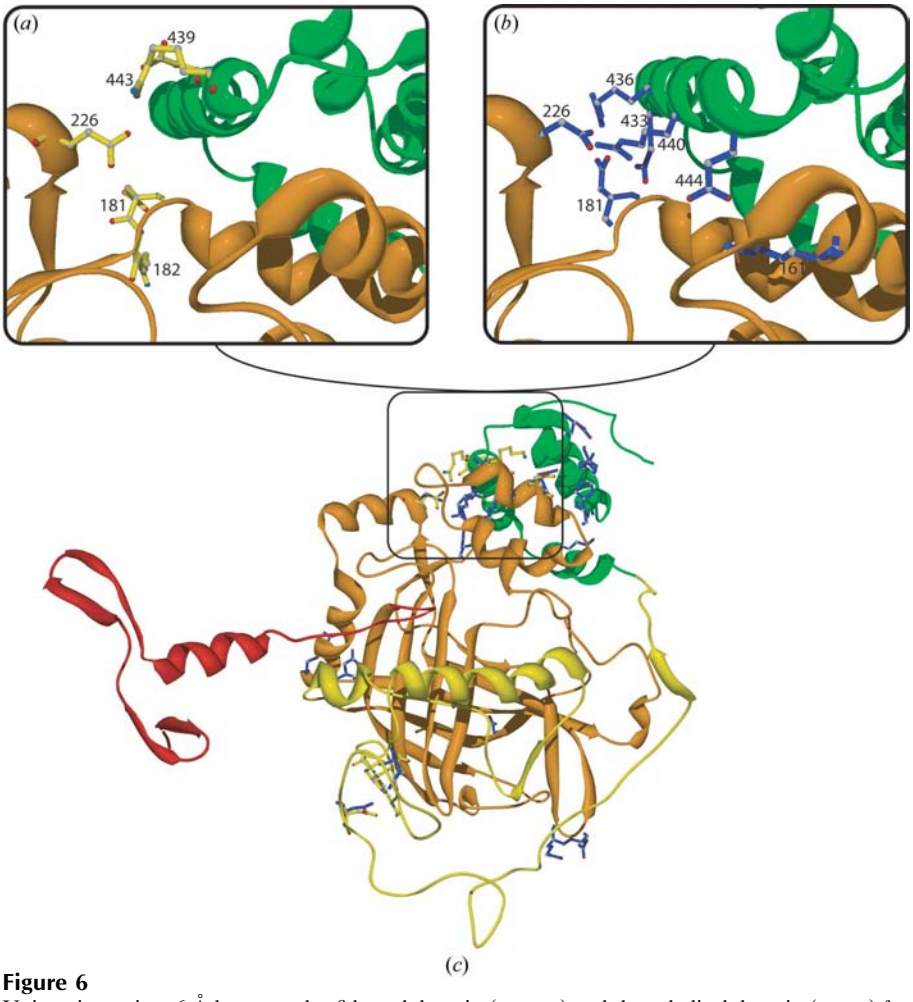

Figure 6
Unique ion pairs <6 Å between the β-barrel domain (orange) and the α-helical domain (green) for VSC (*a*) and PMC (*b*). (*c*) Unique ion-pair interactions <4 Å in the VSC and PMC monomers. Yellow indicates unique interactions in VSC, whereas blue indicates unique interactions in PMC.

Table 7
Number of hydrogen bonds in the crystal structures of VSC and PMC monomers and tetramers.

In all calculations, only the protein atoms are included. Before the calculations were performed, the following double conformations were deleted: Arg99 *ABCD*, Asp478 *A*, Ser378 *BCD* in VSC and Arg99 in PMC. VSC included 482 residues and PMC 476 residues per monomer. *A*, *B*, *C*, *D*, intramolecular hydrogen bonds in one protein monomer only. *ABCD*, total number of intermolecular and intramolecular hydrogen bonds in one tetramer. Inter, intermolecular interactions. MM, main chain–main chain; MS, main chain–side chain; SS, side chain–side chain.

	VSC						PMC		
Monomers	*A*	*B*	*C*	*D*	*ABCD*	Inter	*A*	*ABCD*	Inter
MM	246	244	245	243	1030	52	235	988	48
MS	138	137	136	137	625	77	129	592	76
SS	62	62	58	62	344	100	68	372	100
Total	446	443	439	442	1999	229	432	1952	224
Total per residue	0.925	0.919	0.911	0.917	1.037	0.119	0.908	1.025	0.118

suggesting that the monomers in the psychrotrophic and mesophilic *Vibrio* enzymes are more stabilized compared with the psychrophilic VSC (Table 6).

VSC has six unique ion pairs <4 Å between monomers *A* and *B* (Asp33*A*/*B*–His409*B*/*A*, Glu414*A*/*B*–Lys25*B*/*A* and Asp249*A*/*B*–Arg152*B*/*A*, where *A*/*B*–*B*/*A* indicates two interactions *A*–*B* and *B*–*A*) and two additional unique ion pairs (Lys159*A*/*D*–Asp386*D*/*A*), while PMC has two unique ion pairs (Asp16*A*/*B*–His409*B*/*A*) <4 Å.

When considering distances shorter than 6 Å, VSC has eight unique ion pairs (Glu98*A*/*B*–Arg99*B*/*A*, Glu414*A*/*B*–Lys25*B*/*A*, Arg26*C*–Glu414*D*, Glu392*A*–His16*C* and Asp386*A*/*D*–Lys159*D*/*A*), while PMC has two unique ion pairs (Asp16*A*/*B*–His409*B*/*A*). PMC has no unique ion pairs between these monomers at a 6 Å cutoff.

Monomers *A* and *B* are responsible for dimerization by hooking the N-terminal arm of one monomer through the long wrapping loop around the other monomer (Putnam *et al.*, 2000). The ionic interactions suggest that VSC dimers are slightly more stable than those of PMC. Thus, it appears that the potentially more flexible monomer of VSC is compensated by a more stabilized tetramer. The homology models of the psychrotrophic VFC and the mesophilic VPC seem to support the tendency towards decreased intrasubunit ionic interactions within the monomers and increased intersubunit (between the monomers) ionic interactions from the psychrophilic VSC to the mesophilic PMC (Table 6). The ionic interaction pattern observed in VSC may therefore be a true cold-adaptation strategy for catalases, although to our knowledge such features have not been reported previously for other cold-adapted enzymes.

3.9. Hydrogen bonds

One single hydrogen bond can contribute to the total protein stabilization by 4–12 kJ mol^{-1} (Smalås *et al.*, 2000) and since proteins are only marginally stable, with a net stability difference (ΔG) between the native and unfolded state of 21–63 kJ mol^{-1} (Savage *et al.*, 1993), a few differences in the hydrogen-bonding pattern might have a drastic impact on protein stability. A smaller number of intradomain (between the domains in one monomer) hydrogen bonds is one of the factors suggested to be involved in the reduced stability of cold-adapted trypsins compared with mesophilic trypsins (Leiros *et al.*, 2003). A total of 439–446 hydrogen bonds were identified in the VSC monomers and 432 in PMC (Table 7). In one tetramer there are 47 additional bonds in VSC compared with PMC, where differences in main-chain–main-chain interactions mainly account for the enhancement in VSC. A structural comparison of the backbone residues of VSC and PMC revealed that in many cases PMC residues have slightly different conformations and hence do not fulfill the angle criteria given to *HBPLUS* (McDonald & Thornton, 1994) and are therefore not defined and counted as a satisfactory hydrogen bond. This is also the case for some bonds found to be present in PMC and not in VSC. The models of VFC and VPC were not subjected to a hydrogen-bonding analysis since the calculations are very sensitive and the homology models are less accurate than the VSC and PMC crystal structures. The differences are quite small, but still it appears that the VSC monomer is held together by slightly more hydrogen bonds compared with PMC and the VSC monomers are connected with slightly more intersubunit bonds (five more) than in PMC. This conclusion is also the case if the number of hydrogen bonds per residue are calculated (Table 7).

4. Conclusion

The crystal structure of VSC reported here is the first structure to be reported for a cold-adapted catalase. Our recent biochemical characterization revealed that the catalase from the psychrophilic marine bacterium *V. salmonicida* (VSC) is two times more catalytically efficient at 277 K compared with the catalase from the mesophilic human pathogen *P. mirabilis* (PMC; Lorentzen *et al.*, 2006). Furthermore, VSC showed a lower temperature optimum for activity and a lower thermal stability compared with PMC, with a half-life at 333 K of <5 min for VSC compared with 50 min for PMC and a 19 K lower T_m. The driving force for solving the crystal structure of VSC was to possibly explain at a detailed atomic level the observed typical cold-adaptation features: high enzymatic activity and low thermal stability.

The crystal structure of VSC suggests that the enhanced, nearly diffusion-controlled degradation of hydrogen peroxide into water and molecular oxygen in VSC compared with PMC could be a consequence of smaller sized residues and a reduced number of hydrogen bonds in the haem-binding site, thus causing increased local flexibility in VSC which could explain the biochemical results. Increased channel diameter and fewer ion-pair interactions and hydrogen bonds within the major channel may also facilitate easier access of the substrate

to the active site and to the haem group in VSC than in PMC. The same would also be applicable for the leaving products.

Possible explanations for the lower thermal stability of VSC are a slightly lower number of ion pairs in the monomers and fewer residues involved in ion-pair networks. Particularly interesting are the missing ion-pair interactions from helices α9–α12 in the α-helical domain to the β-barrel domain in VSC. These interactions might explain the displacement of the helix bundle in VSC relative to PMC as observed in the crystal structures. Since this domain includes the C-terminus of the protein, this could be an unfolding initiation site in VSC. Destabilization of termini in other cold-adapted proteins has been proposed to be responsible for reduced thermal stability (Leiros *et al.*, 2000). The VSC tetramer seems to be slightly more stabilized by intersubunit ion-pair interactions than that in PMC. To our knowledge, a reduced number of intradomain ion pairs combined with a higher number of intersubunit ion-pair interactions have not been observed previously in other cold-adapted enzymes.

The present crystal structure of a cold-adapted catalase supports the theory that every psychrophilic enzyme has its own way of adapting to lower environmental temperatures. However, in order to find the true nature of cold adaptation of catalase from *V. salmonicida* and to obtain more detailed knowledge about the factors correlating flexibility, stability and catalytic activity, mutational studies in combination with kinetic data need to be carried out. The structures should also be subjected to molecular-dynamics studies.

We gratefully acknowledge Dr Sigrun Espelid and Dr Elin Moe, NorStruct, Department of Chemistry, University of Tromsø, Norway for assistance with the present manuscript. This work was supported by The Norwegian Research Council (grant 143450/140) and by the National Functional Genomics Programme (FUGE) from The Research Council of Norway. Provision of beamtime at the Swiss Light Source (SLS) and Swiss–Norwegian Beamline (SNBL) at the European Synchrotron Radiation Facility (ESRF) is gratefully acknowledged.

References

Almarsson, O., Sinha, A., Gopinath, E. & Bruice, T. C. (1993). *J. Am. Chem. Soc.* **115**, 7093–7102.
Amara, P., Andreoletti, P., Jouve, H. M. & Field, M. J. (2001). *Protein Sci.* **10**, 1927–1935.
Bicout, D. J., Field, M. J., Gouet, P. & Jouve, H. M. (1995). *Biochim. Biophys. Acta*, **1252**, 172–176.
Bravo, J., Verdaguer, N., Tormo, J., Betzel, C., Switala, J., Loewen, P. C. & Fita, I. (1995). *Structure*, **3**, 491–502.
Buzy, A., Bracchi, V., Sterjiades, R., Chroboczek, J., Thibault, P., Gagnon, J., Jouve, H. M. & Hudry-Clergeon, G. (1995). *J. Protein Chem.* **14**, 59–72.
Carpena, X., Soriano, M., Klotz, M. G., Duckworth, H. W., Donald, L. J., Melik-Adamyan, W., Fita, I. & Loewen, P. C. (2003). *Proteins*, **50**, 423–436.
Chelikani, P., Fita, I. & Loewen, P. C. (2004). *Cell. Mol. Life Sci.* **61**, 192–208.
Collaborative Computational Project, Number 4 (1994). *Acta Cryst.* D**50**, 760–763.
D'Amico, S., Claverie, P., Collins, T., Georlette, D., Gratia, E., Hoyoux, A., Meuwis, M. A., Feller, G. & Gerday, C. (2002). *Philos. Trans. R. Soc. London Ser. B Biol. Sci.* **357**, 917–925.
DeLano, W. L. (2002). *The PyMol Molecular Graphics System.* http://www.pymol.org.
DeLuca, D. C., Dennis, R. & Smith, W. G. (1995). *Arch. Biochem. Biophys.* **320**, 129–134.
Fita, I. & Rossmann, M. G. (1985). *J. Mol. Biol.* **185**, 21–37.
Fita, I., Silva, A. M., Murthy, M. R. N. & Rossmann, M. G. (1986). *Acta Cryst.* B**42**, 497–515.
Gianese, G., Argos, P. & Pascarella, S. (2001). *Protein Eng.* **14**, 141–148.
Gianese, G., Bossa, F. & Pascarella, S. (2002). *Proteins*, **47**, 236–249.
Gouet, P., Courcelle, E., Stuart, D. I. & Metoz, F. (1999). *Bioinformatics*, **15**, 305–308.
Gouet, P., Jouve, H. M. & Dideberg, O. (1995). *J. Mol. Biol.* **249**, 933–954.
Gudmundsdottir, E., Spilliaert, R., Yang, Q., Craik, C. S., Bjarnason, J. B. & Gudmundsdottir, A. (1996). *Comput. Biochem. Physiol. B Biochem. Mol. Biol.* **113**, 795–801.
Guex, N. & Peitsch, M. C. (1997). *Electrophoresis*, **18**, 2714–2723.
Håkansson, K. O., Brugna, M. & Tasse, L. (2004). *Acta Cryst.* D**60**, 1374–1380.
Hillar, A. & Nicholls, P. (1992). *FEBS Lett.* **314**, 179–182.
Hillar, A., Nicholls, P., Switala, J. & Loewen, P. C. (1994). *Biochem. J.* **300**, 531–539.
Hochachka, P. W. & Somero, G. N. (1984). *Biochemical Adaptations.* Princeton: Princeton University Press.
Jones, T. A., Zou, J.-Y., Cowan, S. W. & Kjeldgaard, M. (1991). *Acta Cryst.* A**47**, 110–119.
Kabsch, W. & Sander, C. (1983). *Biopolymers*, **22**, 2577–2637.
Kalko, S. G., Gelpi, J. L., Fita, I. & Orozco, M. (2001). *J. Am. Chem. Soc.* **123**, 9665–9672.
Kim, S.-Y., Hwang, K. Y., Kim, S.-H., Sung, H.-C., Han, Y. S. & Cho, Y. (1999). *J. Biol. Chem.* **274**, 11761–11767.
Kirkman, H. N., Galiano, S. & Gaetani, G. F. (1987). *J. Biol. Chem.* **262**, 660–666.
Kirkman, H. N., Rolfo, M., Ferraris, A. M. & Gaetani, G. F. (1999). *J. Biol. Chem.* **274**, 13908–13914.
Laskowski, R. A., MacArthur, M. W., Moss, D. S. & Thornton, J. M. (1993). *J. Appl. Cryst.* **26**, 283–291.
Leiros, I., Moe, E., Lanes, O., Smalås, A. O. & Willassen, N. P. (2003). *Acta Cryst.* D**59**, 1357–1365.
Leiros, H. K., Willassen, N. P. & Smalås, A. O. (2000). *Eur. J. Biochem.* **267**, 1039–1049.
Loewen, P. C., Carpena, X., Rovira, C., Ivancich, A., Perez-Luque, R., Haas, R., Odenbreit, S., Nicholls, P. & Fita, I. (2004). *Biochemistry*, **43**, 3089–3103.
Lorentzen, M. S., Moe, E., Jouve, H. M. & Willassen, N. P. (2006). *Extremophiles*, **10**, 427–440.
Luzzati, V. (1952). *Acta Cryst.* **5**, 802–810.
McCoy, A. J., Grosse-Kunstleve, R. W., Storoni, L. C. & Read, R. J. (2005). *Acta Cryst.* D**61**, 458–464.
McDonald, I. K. & Thornton, J. M. (1994). *J. Mol. Biol.* **238**, 777–793.
Maté, M., Murshudov, G., Bravo, J., Melik-Adamyan, V. R., Loewen, P. C. & Fita, I. (2001). *Handbook of Metalloproteins*, edited by A. Messerschmidt, R. Huber, T. Poulos & K. Wieghardt, pp. 486–502. Chichester: Wiley.
Melik-Adamyan, W. R., Barynin, V. V., Vagin, A. A., Borisov, V. V., Vainshtein, B. K., Fita, I., Murthy, M. R. & Rossmann, M. G. (1986). *J. Mol. Biol.* **188**, 63–72.
Murshudov, G. N., Grebenko, A. I., Brannigan, J. A., Antson, A. A., Barynin, V. V., Dodson, G. G., Dauter, Z., Wilson, K. S. & Melik-Adamyan, W. R. (2002). *Acta Cryst.* D**58**, 1972–1982.
Murshudov, G. N., Melik-Adamyan, W. R., Grebenko, A. I., Barynin,

V. V., Vagin, A. A., Vainshtein, B. K., Dauter, Z. & Wilson, K. S. (1992). *FEBS Lett.* **312**, 127–131.
Murshudov, G. N., Vagin, A. A. & Dodson, E. J. (1997). *Acta Cryst.* D**53**, 240–255.
Nicholls, P., Fita, I. & Loewen, P. C. (2001). *Adv. Inorg. Chem.* **51**, 51–106.
Ossowski, I. von, Hausner, G. & Loewen, P. C. (1993). *J. Mol. Evol.* **37**, 71–76.
Putnam, C. D., Arvai, A. S., Bourne, Y. & Tainer, J. A. (2000). *J. Mol. Biol.* **296**, 295–309.
Riise, E. K., Lorentzen, M. S., Helland, R. & Willassen, N. P. (2006). *Acta Cryst.* F**62**, 77–79.
Russell, N. J. (2000). *Extremophiles*, **4**, 83–90.
Russell, R. J., Gerike, U., Danson, M. J., Hough, D. W. & Taylor, G. L. (1998). *Structure*, **6**, 351–361.
Savage, H., Elliot, C., Freeman, C. & Finney, J. (1993). *J. Chem. Soc. Faraday Trans.* **89**, 2609–2617.
Sheridan, P. P., Panasik, N., Coombs, J. M. & Brenchley, J. E. (2000). *Biochim. Biophys. Acta*, **1543**, 417–433.
Smalås, A. O., Leiros, H. K., Os, V. & Willassen, N. P. (2000). *Biotechnol. Annu. Rev.* **6**, 1–57.
Switala, J. & Loewen, P. C. (2002). *Arch. Biochem. Biophys.* **401**, 145–154.
Thompson, J. D., Plewniak, F., Thierry, J. & Poch, O. (2000). *Nucleic Acids Res.* **28**, 2919–2926.
Vaguine, A. A., Richelle, J. & Wodak, S. J. (1999). *Acta Cryst.* D**55**, 191–205.
Vriend, G. (1990). *J. Mol. Graph.* **8**, 52–56, 29.
Zamocky, M. & Koller, F. (1999). *Prog. Biophys. Mol. Biol.* **72**, 19–66.